

Striped nanoscale phase separation at the metal-insulator transition of heteroepitaxial nickelates

G. Mattoni,¹ P. Zubko,² F. Maccherozzi,³ A.J.H. van der Torren,⁴ D.B. Boltje,⁴ M. Hadjimichael,² N. Manca,¹ S. Catalano,⁵ M. Gibert,⁵ Y. Liu,³ J. Aarts,⁴ J.-M. Triscone,⁵ S.S. Dhesi,³ and A.D. Caviglia¹

¹*Kavli Institute of Nanoscience, Delft University of Technology, Netherlands*

²*University College London, London Centre for Nanotechnology, UK*

³*Diamond Light Source, Chilton, Didcot, UK*

⁴*Huygens-Kamerlingh Onnes Laboratory, Leiden University, Netherlands*

⁵*DQMP University of Geneva, Switzerland*

(Dated: December 3, 2024)

Nucleation processes of mixed-phase states are an intrinsic characteristic of first-order phase transitions, typically related to local symmetry breaking. Direct observation of emerging mixed-phase regions in materials showing a first-order metal-insulator transition (MIT) offers unique opportunities to understand their intrinsic properties. Using photoemission electron microscopy (PEEM), we image the nanoscale formation and growth of insulating domains across the temperature-driven MIT in NdNiO_3 epitaxial thin films. Heteroepitaxy is found to strongly determine the nanoscale nature of the phase transition, inducing preferential formation of striped domains along the terraces of atomically flat stepped surfaces. We show that the distribution of transition temperatures is an intrinsic local property, set by surface morphology and stable across multiple temperature cycles. Our data provides new insights into the MIT in nickelates and points to a rich, nanoscale phenomenology in this strongly correlated material.

Rare-earth nickelates are strongly correlated electron systems in which structural and electronic properties are interconnected [1, 2]. A well-studied member of this family is NdNiO_3 , which shows a first order temperature-driven metal-insulator transition (MIT) accompanied by a structural phase change as well as unconventional magnetic order [3–6]. Several models have been proposed to describe its electronic structure, however the microscopic mechanism of the phase transition is still debated [7–13]. A number of experiments underscore the key role of the lattice, as demonstrated by the influence of hydrostatic pressure, epitaxial strain and resonant phonon excitation on the MIT [14–23]. The coexistence of metallic and insulating regions in the vicinity of the MIT, typical of first order phase transitions, has been discussed with an expected domain size of a few tens of nanometre [16, 24]. However, the formation of the insulating phase has been inferred, so far, mainly from macroscopic transport measurements [25–27]. In such thermodynamic limit the influence of nanoscale control parameters, such as local strain fields, lattice distortions and inhomogeneity, is buried in the statistical average of multiple domains. Fundamental understanding and control of phase separation, necessary for the development of nanoscale oxide electronics [28, 29], requires access to the nanoscale regime.

In the present work we show that heteroepitaxy of NdNiO_3 on atomically flat stepped surfaces leads to striped domain nucleation and growth along surface terraces across the MIT. We discuss how morphological characteristics act as a template for phase separation, determining a persistent shift of the local transition temperature, as well as domain nucleation and growth pathways.

Our data evidences, for the first time in the nanometre range, the strong coupling between structural and electronic degrees of freedom in the rare-earth nickelates.

Several methodologies have been employed to image mixed metallic and insulating phases in correlated oxides such as scanning tunnelling microscopy [30], near-field infrared microscopy [31] and scanning electron microscopy [32]. Here we use photoemission electron microscopy (PEEM) to image the evolution of NdNiO_3 MIT at the local scale. Our technique combines nanometre spatial resolution with real-time imaging, allowing us to track the phase transition at different stages of its evolution.

RESULTS

Sample characterisation

For this experiment a 30 unit-cells thick NdNiO_3 (001) epitaxial film was grown on a NdGaO_3 substrate. The epitaxial strain imposed by the substrate sets the transition temperature span for the MIT and the width of the hysteresis loop [17]. As shown in the atomic force microscopy (AFM) measurement of fig. 1a, the film presents an atomically flat surface with steps and terraces that mimic the underlying substrate. The inset of fig. 1b shows a θ - 2θ X-ray diffraction (XRD) scan around the (001) peak of the NdNiO_3 film. Finite size oscillations are observed and fitted with a kinematic scattering model, indicating high crystalline quality and confirming the expected film thickness.

The MIT hysteresis, associated with the formation of insulating domains, is measured by four probe DC

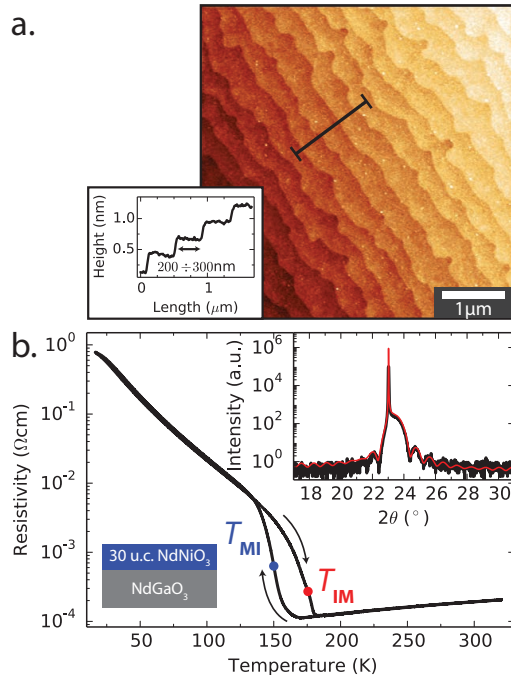


FIG. 1. Characterisation of the 30 unit cell thick NdNiO_3 film. (a) Surface morphology with single unit cell steps (0.4 nm) and terraces (200 nm to 300 nm in width) as measured by atomic force microscopy. Inset: cross-section profile showing the film steps height. (b) Resistance versus temperature from the transport measurement, where T_{MI} (blue dot) and T_{IM} (red dot) are indicated as extracted from the peaks of $-\partial \log R / \partial T$. In the inset, X-ray diffraction data (black) around NdNiO_3 (001) peak, fitted with a kinematic scattering model (red).

transport (fig. 1b). We define the transition temperatures $T_{\text{MI}} = 150 \text{ K}$ and $T_{\text{IM}} = 178 \text{ K}$ as the peaks of $-\partial \log R / \partial T$ during a cooling and warming cycle, respectively. The hysteresis width is thus calculated from the peaks separation as $\Delta T_{\text{MIT}} = 28 \text{ K}$. In agreement with previous reports [16], the MIT width in thin films appears much broader than in bulk NdNiO_3 , signalling the influence of epitaxy on the phase transition evolution.

Imaging contrast mechanism

To image the different electronic phases, we first perform X-ray absorption spectroscopy (XAS) at Ni L_3 absorption edge. We use linear- σ X-ray polarisation and acquire the signal in total electron yield (TEY), thus probing the material surface down to a few sub-surface atomic layers. In fig. 2a the temperature dependence of the Ni L_3 XAS is presented. The most intense absorption peak shifts towards lower photon energies upon cooling the sample from the metallic state at $T = 185 \text{ K}$ to the insulating state at $T = 140 \text{ K}$. This energy shift provides

a contrast mechanism suitable for our study.

Above the MIT, the XAS spectra measured over the full field of view do not display significant variations compared to the noise level of the experiment. Below the MIT, instead, the sample shows different spatially-dependent XAS spectra, divided in two subsets with a relative shift in absorption edge (fig. 2c). The maximum difference between the two subsets spectra is observed at 852.0 eV and 852.7 eV. We thus construct electronic phase maps by acquiring PEEM images at these two photon energies, and calculate their difference pixel-by-pixel. In all images a round-shaped surface defect (dashed square) provides a well-contrasted reference feature used to compensate for the time-dependent spatial drift and keep the same area of interest in focus during the experiment.

At $T = 185 \text{ K}$ the resulting map (fig. 2b) is spatially homogeneous, while at $T = 140 \text{ K}$ alternating bright and dark features (fig. 2d) appear. We identify the bright features as insulating domains nucleating in a metallic matrix during the metal-insulator transition. Indeed, as shown in fig. 2c, the bright features display local spectra that are shifted to lower energies when compared to the dark ones. Such shift is in agreement with the spatially averaged XAS spectra of fig. 2a measured above and below the transition temperature.

If we compare the PEEM and AFM measurements ac-

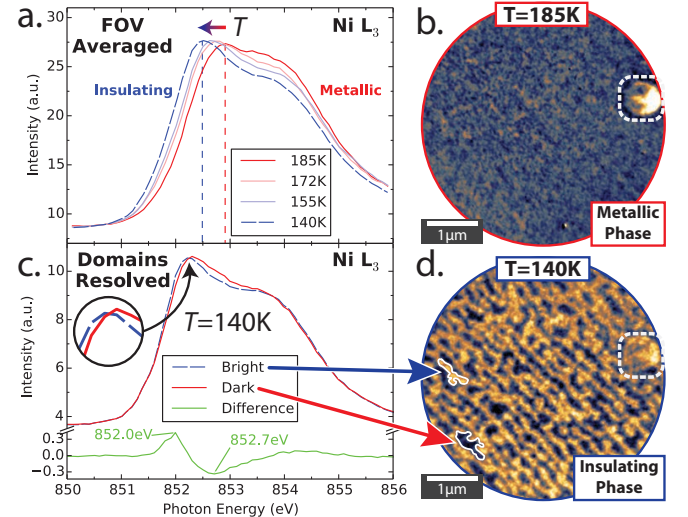


FIG. 2. The PEEM imaging contrast from photon-energy-shifted XAS spectra of metallic and insulating phases. (a) Temperature dependence of Ni L_3 XAS spectra measured over the full field of view. PEEM images of (b) high temperature metallic phase and (d) low temperature insulating phase. A surface defect used as a reference feature for drift-correction is indicated by the dashed square. (c) Domains resolved XAS spectra of bright and dark features in panel (d).

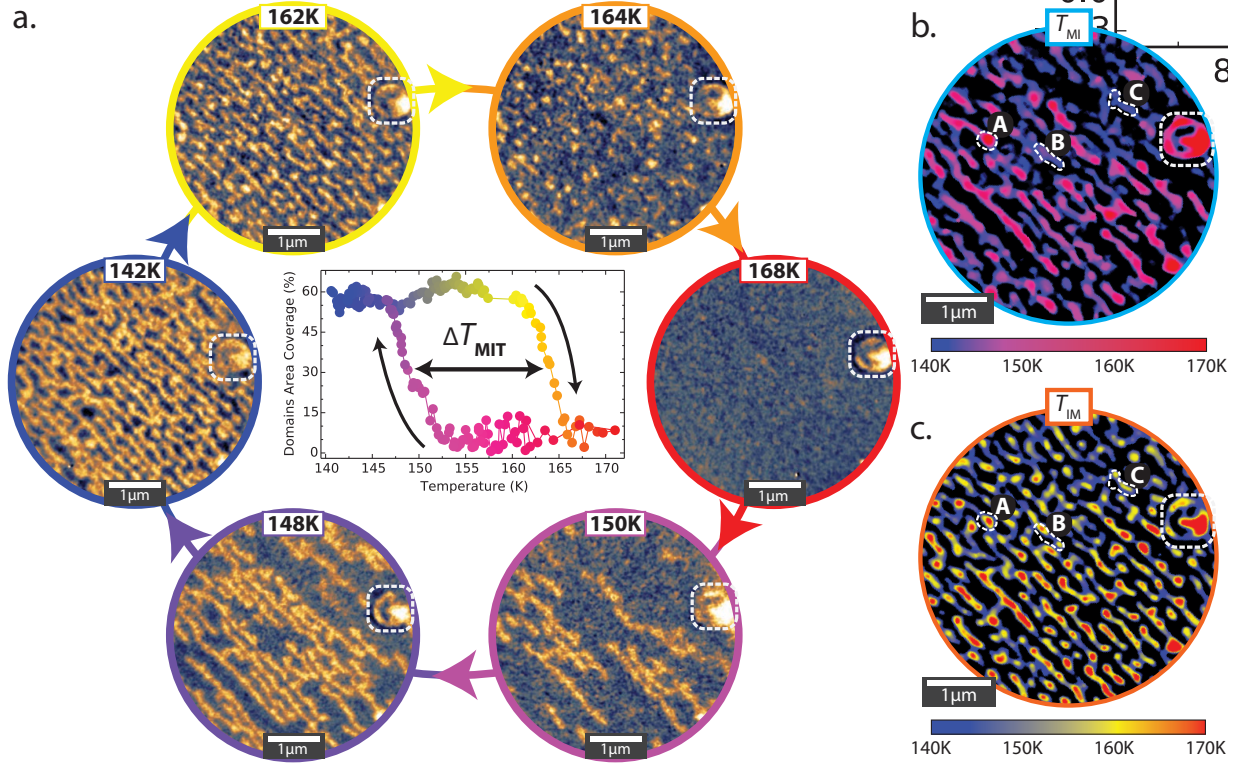


FIG. 3. Temperature evolution of insulating domains across the MIT. (a) During each thermal cycle the insulating domains nucleate and grow with decreasing temperature, while they gradually disappear with increasing temperature (see video in the supplementary material). The inner panel shows the percentage of image area covered by the insulating domains as a function of temperature, highlighting the hysteretic behaviour of the MIT and an estimation of the single-domain hysteresis width. Spatial maps of (b) T_{MI} and (c) T_{IM} showing the transition temperature is an intrinsic local property of the material. Three areas are encircled to indicate the order with which they become insulating (A,B,C) and revert to the metallic state (C,B,A).

quired with the same sample orientation (figs. 1a and 2d), we find a direct relationship between the insulating domains and surface morphology. The surface terraces act as nucleation centres for the insulating phase [24], so that insulating domains form and grow preferentially along the terraces, resulting in a striped shape. This observation has been reproduced on 3 different samples, confirming the domains direction and size is dictated by surface morphology (see supplementary information). Our finding establishes an important link between sample local morphology and electronic phase separations.

Nanoscale evolution of the MIT

In order to investigate the evolution of the insulating domains across the MIT, sample temperature is cycled below and above the transition, following the hysteresis loop. A representative set of images is reported in fig. 3a. From each PEEM image of the series the percentage of area covered by the insulating domains is evaluated (inset of fig. 3a). From room temperature down to 152 K

the sample shows a homogeneous metallic phase. Below 152 K insulating domains nucleate and grow along the preferential direction given by surface terraces, gradually forming striped regions. Between 146 K and 140 K the domain evolution saturates at about 60% coverage and no additional insulating regions are formed. This domain configuration is stable for the whole duration of the measurements (several hours).

The reverse transition, back to the metallic state, is rather different. Upon warming up, no change is initially observed up to 161 K, in agreement with the hysteretic, first-order nature of NdNiO_3 MIT. Above 161 K the insulating stripes become narrower and are pinched off into several sparse nano-domains by the expanding metallic matrix. These appear to be evenly distributed across the field of view, in stark contrast to the striped domains observed on cooling (i.e. compare the fig. 3a heating and cooling images at 164 K and 150 K, respectively, with approximately the same insulating domains coverage). At $T = 165$ K all the insulating domains disappear and the homogeneous metallic phase is recovered. Interestingly, we note that the insulating domains do not fully populate

the surface as the area coverage reaches the saturation value of about 60%. We observe no significant variation of the coverage down to 130 K. The domains are often spaced by metallic regions, which persist at the surface step edges. This effect can be related either to local strain fields in proximity of the step edges or to inhomogeneous surface termination.

The observed evolution is consistent across multiple temperature cycles. This allows us to assign local transition temperatures to the material. In figs. 3b and 3c we present spatially resolved maps of local T_{MI} and T_{IM} , showing the temperature at which the phase transition occurs on a certain region of the sample. Repeating the temperature cycle several times, the insulating domains are observed nucleating and growing always in the same position and in the same order. As an example we considered the areas labelled as A, B and C in figs. 3b and 3c. If upon a cool-down cycle they turn insulating in an (A, B, C) order, during a warm-up they will revert to the metallic state in the reversed (C, B, A) order.

A relevant information that we can extract from our analysis is the hysteresis width of a single domain. Since the MIT evolution measured at the nanoscale has a discrete character, we can track down the switching of single domains and estimate $\Delta T_{MIT} = (14 \pm 2)$ K, in sharp contrast with bulk transport measurements. We also note that the observed nanoscale inhomogeneities appear on a smaller length scale than the field of view used in the experiment, thus providing a representative evaluation of the properties of the material. The existence of a finite hysteresis width down to the single domain scale, and the spatial distribution of T_{MI} and T_{IM} provide a further insight in the nature of the phase transition. Such results can hardly be inferred by macroscopic measurements which are subject to statistical averaging.

MIT through bulk and surface techniques

At this point it is worth comparing the temperature dependence of the domain area coverage measured by PEEM with the resistivity data, both shown in fig. 4, magnified on the relevant temperature range. We see a striking difference in the extremal temperatures of the two hysteresis loops. In the PEEM data the hysteresis loop closes at 165 K on the high temperature end, about 15 K lower than in the transport case. This means that while the insulating domains coverage goes to zero at 165 K during a warming ramp, the resistivity is still almost an order of magnitude higher than in the metallic state. Assuming the domain structures propagate completely through the film thickness (i.e. that 0% area coverage also corresponds to 0% volume fraction), it is not possible to explain the difference between area coverage and transport.

In order to get a further insight into this difference, we

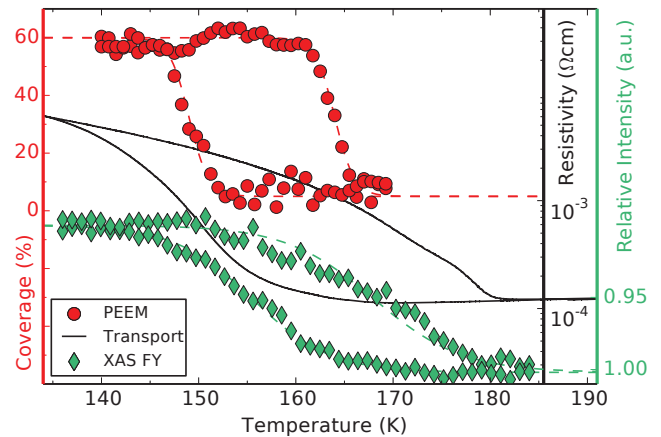


FIG. 4. Metal-insulator transition hysteresis measured with different techniques. Insulating domains area coverage from the inset of fig. 3a (red dots), low temperature transport from fig. 1b (black line), and X-ray absorption intensity at 853 eV photon energy relative to the intensity at 180 K measured in fluorescence yield (green diamonds).

additionally measure the evolution of macroscopic XAS intensity at 853 eV in the fluorescence yield (FY) configuration as a function of temperature (green diamonds in fig. 4). The MIT hysteresis measured this way is in qualitative agreement with the transport data. In contrast to the measurements in total electron yield (TEY) performed in the PEEM setup, the XAS in FY probes the whole thickness of our NdNiO_3 thin film, also providing a more extended spatial averaging as the X-rays spot size is about two orders of magnitude larger.

A possible explanation for the measured discrepancy between PEEM and transport/XAS is that the observed domain structures do not penetrate throughout the whole film but are, instead, confined to the surface. In this case, our measurements indicate that the MIT at the surface occurs at a lower temperature than in the bulk. Additional experiments, such as transport measurements at the nanoscale, are required to get further insights into this still open question.

DISCUSSION

Through direct imaging by PEEM, we reported on nanoscale phase separation during the metal-insulator transition of NdNiO_3 thin films. Striped domains nucleate and grow along the terraces of the atomically flat surface, highlighting the influence of heteroepitaxy on the phase transition. Performing a systematic imaging as a function of temperature, we showed that the transition temperature is an intrinsic local property of the material, stable across multiple temperature cycles. We could estimate that single domains have a finite hysteresis width of $\Delta T_{MIT} = (14 \pm 2)$ K, indicating the hysteresis per-

sists down to a single domain. Comparing PEEM with transport and XAS in FY, we found a discrepancy in the MIT extremal temperatures measured with surface and bulk techniques. Our data indicates the observed domain structures might be confined to the surface, a question to be investigated in future studies. Our measurements point towards a strong interconnection between structural and electronic degrees of freedom in rare-earth nickelates, suggesting a new approach for controlling phase separation at the nanoscale.

METHODS

The commercially available NdGaO_3 substrate was annealed at 1000°C in 1 atm of oxygen prior to sample growth to achieve a flat surface with a regular step and terrace structure. The NdNiO_3 (001) film was grown by off-axis radio-frequency magnetron sputtering in 1.80×10^{-1} mbar of an oxygen/argon mixture of ratio 1:3 at a substrate temperature of 490°C .

Transport, PEEM and XAS FY measurements have been performed cycling sample temperature at a constant rate of 0.5 K min^{-1} for both ramp directions, guaranteeing the sample is kept in a quasi-static condition.

PEEM and XAS FY data has been acquired at the beamline I06 of Diamond Light Source. An X-ray beam $10 \mu\text{m} \times 10 \mu\text{m}$ in spot size with a fluency of 1 mJ cm^{-2} was used in the PEEM setup, while a $100 \mu\text{m} \times 100 \mu\text{m}$ beam with 0.01 mJ cm^{-2} of fluency was employed for the XAS FY measurements. In both cases the polarisation of the X-rays was linear- σ . The absolute peak photon energies measured by PEEM are subjected to an uncertainty of about 0.2 eV due to the small integration time of 1 s compared to the noise level of the system. However this does not affect the reported data as all PEEM images are based on relative spatial shifts of X-ray absorption intensity.

- [9] H. Park, A. J. Millis, and C. A. Marianetti, *Physical review letters* **109**, 156402 (2012).
- [10] S. Johnston, A. Mukherjee, I. Elfimov, M. Berciu, and G. A. Sawatzky, *Physical review letters* **112**, 106404 (2014).
- [11] W. J. Hardy, H. Ji, E. Mikheev, S. Stemmer, and D. Nettelton, *Physical Review B* **90**, 205117 (2014).
- [12] A. Subedi, O. E. Peil, and A. Georges, *Phys. Rev. B* **91**, 075128 (2015).
- [13] M. H. Upton, Y. Choi, H. Park, J. Liu, D. Meyers, J. Chakhalian, S. Middey, J.-W. Kim, and P. J. Ryan, *Physical review letters* **115**, 036401 (2015).
- [14] X. Obradors, L. Paulius, M. Maple, J. Torrance, A. Nazal, J. Fontcuberta, and X. Granados, *Physical Review B* **47**, 12353 (1993).
- [15] P. Canfield, J. Thompson, S. Cheong, and L. Rupp, *Physical review B* **47**, 12357 (1993).
- [16] G. Catalan, R. Bowman, and J. Gregg, *Physical Review B* **62**, 7892 (2000).
- [17] R. Scherwitzl, P. Zubko, I. G. Lezama, S. Ono, A. F. Morpurgo, G. Catalan, and J.-M. Triscone, *Advanced Materials* **22**, 5517 (2010).
- [18] A. Caviglia, R. Scherwitzl, P. Popovich, W. Hu, H. Bromberger, R. Singla, M. Mitrano, M. Hoffmann, S. Kaiser, P. Zubko, *et al.*, *Physical review letters* **108**, 136801 (2012).
- [19] P.-H. Xiang, N. Zhong, C.-G. Duan, X. Tang, Z. Hu, P. Yang, Z. Zhu, and J. Chu, *Journal of Applied Physics* **114**, 243713 (2013).
- [20] J. Liu, M. Kargarian, M. Kareev, B. Gray, P. J. Ryan, A. Cruz, N. Tahir, Y.-D. Chuang, J. Guo, J. M. Rondinelli, *et al.*, *Nature communications* **4** (2013).
- [21] S. Catalano, M. Gibert, V. Bisogni, F. He, R. Sutarto, M. Viret, P. Zubko, R. Scherwitzl, G. Sawatzky, T. Schmitt, *et al.*, *APL Materials* **3**, 062506 (2015).
- [22] M. Forst, A. D. Caviglia, R. Scherwitzl, R. Mankowsky, P. Zubko, V. Khanna, H. Bromberger, S. B. Wilkins, Y.-D. Chuang, W. S. Lee, W. F. Schlotter, J. J. Turner, G. L. Dakovski, M. P. Minitti, J. Robinson, S. R. Clark, D. Jakusch, J.-M. Triscone, J. P. Hill, S. S. Dhesi, and A. Cavalleri, *Nat Mater* **14**, 883 (2015), letter.
- [23] A. J. Hauser, E. Mikheev, N. E. Moreno, J. Hwang, J. Y. Zhang, and S. Stemmer, *Applied Physics Letters* **106**, 092104 (2015).
- [24] D. Kumar, K. Rajeev, A. Kushwaha, and R. Budhani, *Journal of Applied Physics* **108**, 063503 (2010).
- [25] S. Asanuma, P.-H. Xiang, H. Yamada, H. Sato, H. Inoue, H. Akoh, A. Sawa, K. Ueno, H. Shimotani, H. Yuan, *et al.*, *Applied Physics Letters* **97**, 142110 (2010).
- [26] J. Son, B. Jalan, A. P. Kajdos, L. Balents, S. J. Allen, and S. Stemmer, *Applied Physics Letters* **99**, 192107 (2011).
- [27] J. Shi, Y. Zhou, and S. Ramanathan, *Nature communications* **5** (2014).
- [28] C. Cen, S. Thiel, J. Mannhart, and J. Levy, *Science* **323**, 1026 (2009).
- [29] R. Jany, C. Richter, C. Woltmann, G. Pfanzelt, B. Förg, M. Rommel, T. Reindl, U. Waizmann, J. Weis, J. A. Mundy, *et al.*, *Advanced Materials Interfaces* **1** (2014).
- [30] M. Fäth, S. Freisem, A. Menovsky, Y. Tomioka, J. Aarts, and J. Mydosh, *Science* **285**, 1540 (1999).
- [31] M. M. Qazilbash, M. Brehm, B.-G. Chae, P.-C. Ho, G. O. Andreev, B.-J. Kim, S. J. Yun, A. Balatsky, M. Maple, F. Keilmann, *et al.*, *Science* **318**, 1750 (2007).

- [1] M. L. Medarde, *Journal of Physics: Condensed Matter* **9**, 1679 (1997).
- [2] G. Catalan, *Phase Transitions* **81**, 729 (2008).
- [3] J. Garcia-Munoz, J. Rodriguez-Carvajal, P. Lacorre, and J. Torrance, *Physical review B* **46**, 4414 (1992).
- [4] J. García-Muñoz, J. Rodriguez-Carvajal, and P. Lacorre, *Physical Review B* **50**, 978 (1994).
- [5] V. Scagnoli, U. Staub, Y. Bodenthin, M. Garcia-Fernandez, A. Mulders, G. Meijer, and G. Hammerl, *Physical Review B* **77**, 115138 (2008).
- [6] A. Caviglia, M. Först, R. Scherwitzl, V. Khanna, H. Bromberger, R. Mankowsky, R. Singla, Y.-D. Chuang, W. Lee, O. Krupin, *et al.*, *Physical Review B* **88**, 220401 (2013).
- [7] T. Mizokawa, D. Khomskii, and G. Sawatzky, *Physical Review B* **61**, 11263 (2000).
- [8] S. Lee, R. Chen, and L. Balents, *Physical Review B* **84**, 165119 (2011).

[32] T.-H. Kim, M. Angst, B. Hu, R. Jin, X.-G. Zhang, J. Wendelken, E. Plummer, and A.-P. Li, *Proceedings of the National Academy of Sciences* **107**, 5272 (2010).

ACKNOWLEDGMENTS

We acknowledge the Foundation for Fundamental Research on Matter (FOM), the Nanofront consortia and NWOnano program funded by the Netherlands Science Foundation NWO/OCW, Diamond Light Source for the provision of beamtime under proposal number SI-13081 and SI-10428. This work was supported by the Swiss National Science Foundation through Division

II and the European Research Council under the European Union's Seventh Framework Program (FP7/2007-2013)/ERC Grant Agreement no. 319286 (Q-MAC).

AUTHOR CONTRIBUTIONS

G.M., P.Z., F.M., A.J.H.T., D.B.B. and M.H. performed the PEEM measurements. G.M. performed the transport and AFM measurements. S.C. and M.G. grew the films and performed the XRD characterisation. S.S.D. and F.M. performed the XAS FY measurements. G.M. analysed the data. G.M., N.M. and A.D.C. wrote the manuscript. A.D.C. conceived and supervised the project. All authors reviewed and edited the manuscript.

Supplementary Information

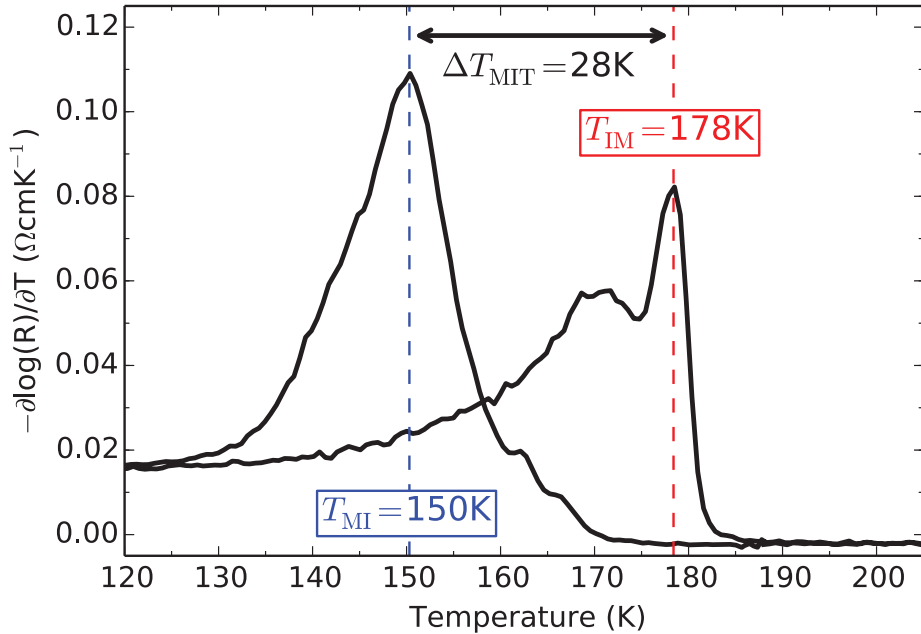


FIG. S1. **Logarithmic derivative of the resistivity from the transport measurement.** The transition temperatures $T_{MI} = 150 \text{ K}$ and $T_{IM} = 178 \text{ K}$ are defined as the peaks of $-\partial \log R/\partial T$ during a cooling and warming cycle, respectively. From the peaks separation the hysteresis width $\Delta T_{MIT} = 28 \text{ K}$ is extracted.

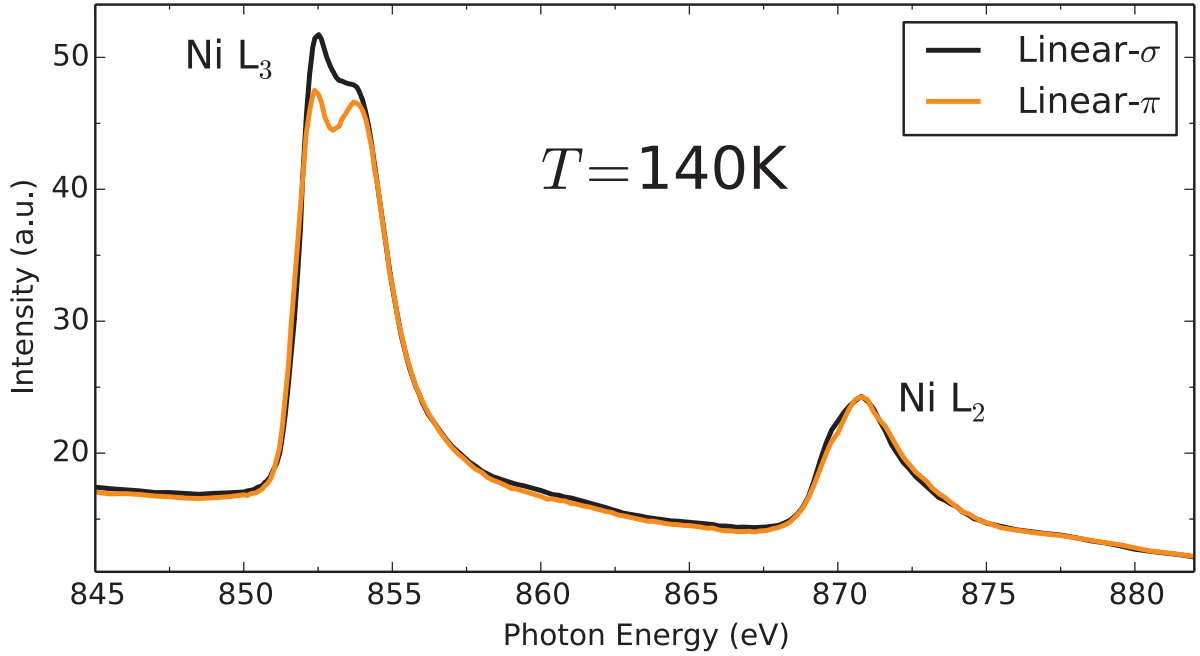


FIG. S2. **Full-range Nickel XAS taken with different X-ray linear polarisations.** A small dichroism in the XAS is observed, stemming from a combined effect of orbital symmetry and charge ordering, consistent with previous reports [Tung et al., Phys. Rev. B 88, 205112 (2013)]. When considering the spatial distribution of dichroic signal measured by PEEM, however, we do not observe any spatial variation compared to our noise level, for any photon energy and sample temperature. As described in the main text for the case of linear- σ polarisation, it is also possible to acquire PEEM measurements at 852.0 eV and 852.7 eV with linear- π polarisation. Calculating their difference pixel-by-pixel, it is possible to construct equivalent PEEM images to the one presented in the main text. We overall used linear- σ polarisation as it provides the most intense absorption peak, thus determining a better signal-to-noise ratio.

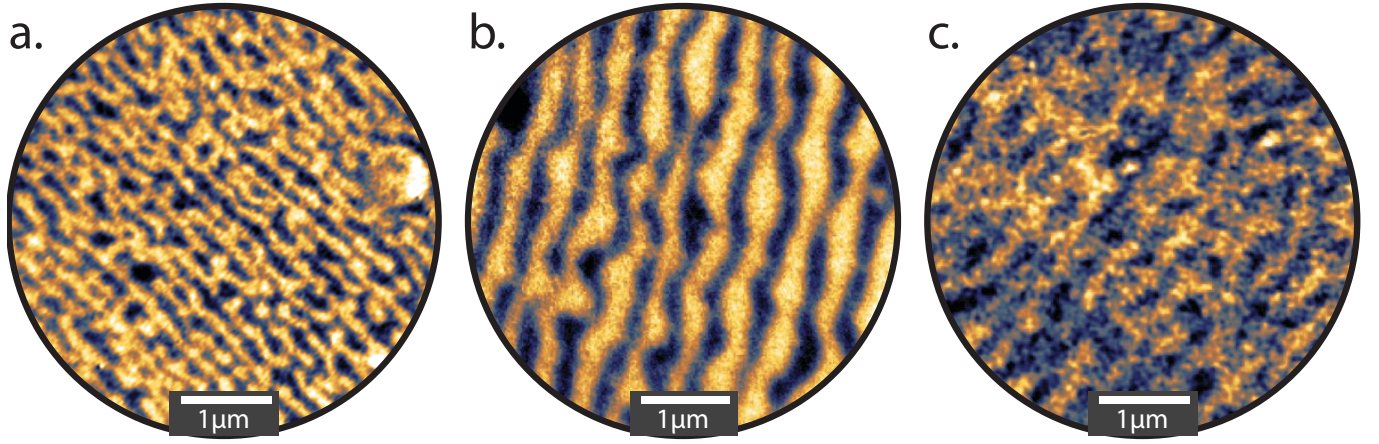


FIG. S3. **PEEM images taken on 3 different samples:** (a) sample discussed in the main text, (b) sample with larger surface terraces, and (c). The insulating domains orientation and size changes from sample to sample according to direction and size of the surface terraces. This remarks the determining contribution of heteroepitaxy in driving the formation of the insulating phase at the metal-insulator transition.